Sustainable Carbon Materials

https://doi.org/10.48130/scm-0026-0011

Original Research

Open Access

Anchoring chitosan on phytic acid-doped polyaniline as capacitive deionization electrodes for uranium capture from wastewater

Chenxiao Hong[1,2], Jing Wang[1,2], Sana Shafi[1,2], Jiayao Hu[1,2], Junyi Chen[2], Ilhom Halimov[3] and Jiaxing Li[1,2*]

Received: 25 December 2025

Revised: 14 January 2026

Accepted: 29 January 2026

Published online: 11 March 2026

Abstract

Capacitive deionization (CDI) has significant potential for the rapid and efficient separation of uranyl ions, although there remains substantial room to improve the development of an appropriate electrode material. Phytic acid-doped polyaniline (PA-PANI) was synthesized in a phytic acid (PA) environment in this work, followed by the immobilization of chitosan on the PA-PANI framework to produce a chitosan-modified spherical material (CS/PA-PANI). Experimental results showed that CS/PA-PANI exhibited much faster kinetics and much higher uranium uptake under applied voltage than systems dominated by either physical or chemical adsorption. UO_2^{2+} adsorption capacity reached a maximum of 942.4 mg g^{-1} at 1.2 V, which is higher than most polymer-based electrodes that have been reported to date. Electrochemical analysis and characterization of the structure suggested that the electroadsorption of UO_2^{2+} on CS/PA-PANI resulted from synergetic effect of capacitive processes and physical-chemical adsorption. The capacitive action was attributed to the formation of electric double layers by polyaniline, whereas the coordination of UO_2^{2+} with the amino or hydroxyl groups accounted for the physico-chemisorption part. This study is a novel and promising polymer electrode on CDI-based extraction of uranium in seawater and nuclear wastewater through integration of rational material design and excellent uranium-capture performance.

Keywords: Uranium capture, Electrosorption, Polyaniline, Phytic acid

Highlights

- A novel uranium-capturing electrode with high adsorption capacity: Chitosan immobilized on phytic acid-doped polyaniline achieved a uranium adsorption capacity of 942.4 mg g^{-1}.
- Synergistic mechanism of electrosorption and chemisorption: Double-layer formation and functional-group coordination synergistically enhance uranium capture efficiency.
- Outstanding selectivity and stability in complex aqueous systems: Efficient uranium removal from seawater and simulated nuclear wastewater with strong interference resistance and reusability.
- Low-energy, low-cost scalable electrode: Energy consumption of only 3.81 Wh kg^{-1}, simple fabrication, suitable for large-scale application.

* Correspondence: Jiaxing Li (lijx@ipp.ac.cn)

Full list of author information is available at the end of the article.

https://doi.org/10.48130/scm-0026-0011

Graphical abstract

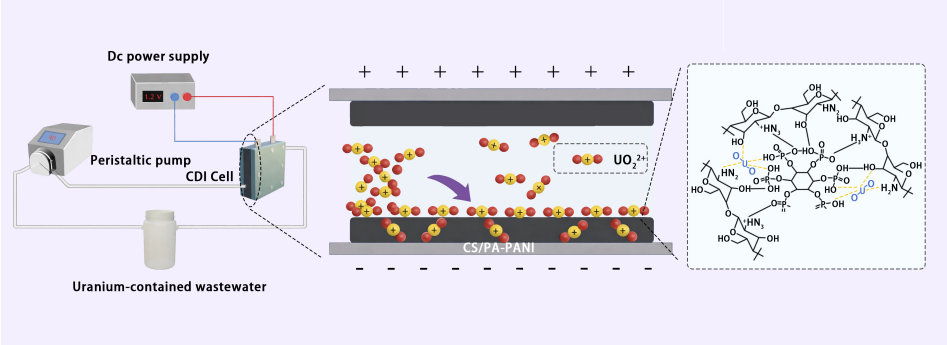

Introduction

As the global demand for energy grows and the climate crisis intensifies, the development of sustainable technologies has become a primary focus for addressing future energy needs[1,2]. Nuclear energy, which is often considered a transitional technology and a bridge between fossil fuels and renewable energy has earned considerable international acclaim on the strategic value[3,4]. Currently, the majority of commercial nuclear reactors utilize uranium as their fission fuel, which is derived from purifying and enriching natural uranium ores with concentrations of around 0.7 per cent uranium[5,6]. Recent estimates by the International Atomic Energy Agency indicate that terrestrial supplies of uranium amount to almost 4.5 million tons, whereas an estimated 4.5 billion tons of dissolved uranium exist in the oceans—a quantity approximately four orders of magnitude greater[7–9]. In addition, seawater content of uranium is constantly replenished, and it is estimated that around 27,000 tons of uranium ions are introduced into the oceans every year via river inputs. Thus, the efficient extraction of uranium from seawater, as well as from nuclear wastewater is essential to the long-term sustainable development of nuclear energy[10].

Various uranium extraction technologies have been developed, such as adsorption[11,12], ion exchange[13,14], membrane separation[15,16], and biological separation[17,18]. Capacitive deionization (CDI) is a promising technology for recovering uranium from aqueous media that has become a promising method in recent years[19,20]. CDI combines the principles of traditional physical and chemical adsorption with electrochemistry: at a low applied voltage, charged ions move to the opposite electrodes, thereby removing ions from the solution[21,22]. The electrostatic interactions between the ions in solution and the porous electrodes enable the storage of ions within the electric double layers (EDLs) formed on the surfaces of porous electrodes, allowing for the effective enrichment of the target species[23]. In addition, the procedure is reversible, and therefore, the target ions can be desorbed when required. An example demonstrating the vast potential of this technique is provided by Wang et al. who reported an amino-functionalized fossil graphene foam (3D FrGOF) electrode, which demonstrated an adsorption capacity of 4,560 mg g^{-1} in 600 mg L^{-1} of uranium solution and lowered the concentration of uranium in simulated seawater, from 3 mg L^{-1} to 19.9 μg L^{-1}[10].

The material used as an electrode is definitely a key determinant of the performance of CDI systems[24]. Consequently, developing effective and economically feasible electrode materials for the elimination of uranyl ions (UO_2^{2+}) is essential[25]. Ideal CDI electrodes should meet four major requirements: high electrical conductivity, large specific surface area, high wettability, and low cost[26]. At present, the majority of CDI electrodes are carbon-based materials, e.g., activated carbon and carbon nanotubes[24,27–30]. Although widely used, these materials usually involve complicated calcination processes and lack specific uranium-binding sites, which limits their selectivity. Conductive polymers have received considerable interest in the recent past as electrode materials due to their high electron conductivity, environmental stability, and straightforward synthesis[31]. For example, to prepare a U(VI) electoadsorption electrode, Yu et al. placed a polyaniline onto biochar to achieve a maximum removal capacity of 282.2 mg g^{-1} under conditions of pH 4.0 and 0.9 V[32]. They also prepared a graphene oxide/polypyrrole composite electrode with a maximum U (VI) uptake of 246.5 mg g^{-1} under similar conditions[33]. Nonetheless, many reported conductive-polymer-based electrodes have comparatively simple structures and low surface areas, limiting the performance of CDI[34]. Proton-acid doping of polyaniline (PANI) is one of the most promising conjugated conductive polymers that can be easily assembled into multifunctional supramolecular structures in a simple, universal, and cheap fashion[35–37]. Its conductivity is high, is environmentally stable, and it can be applied in supercapacitors, batteries, and sensors[38–40]. Through proton-acid doping, the nitrogen atoms in the PANI quinonoid forms are protonated by H^+, and polaronic states are obtained[41,42]. The resulting positive charges delocalize through the conjugated p-system, producing highly conductive carriers along the polymer backbone[43]. Both phytic acid (PA) and chitosan exhibit strong coordination with uranyl ions, thereby enhancing uranium capture efficiency[22,44]. Their affinity towards UO_2^{2+} is also enhanced by their hydrophilia. Leveraging these advantages, we developed a chitosan-functionalized, phytic acid-doped polyaniline system (CS/PA-PANI) for efficient uranium capture via CDI. In this architecture, PANI offers a highly conductive framework and rich routes for transporting UO_2^{2+}, whereas chitosan and PA supply specific coordination sites for uranyl ions. As predicted, CS/PA-PANI demonstrated rapid, efficient, and selective UO_2^{2+} removal via the CDI process, outperforming traditional physical-chemical adsorption. Its overall electrochemical performance, uranium-removal efficacy, and mechanistic analysis confirmed its strong potential.

Experiments

Materials synthesis

Synthesis of PA-PANI

Phytic acid-doped polyaniline (PA-PANI) was synthesized via direct heterogeneous solution polymerization. The standard procedure is as

follows: 0.055 g of MnO_2 was uniformly dispersed in 20 mL of water. Under magnetic stirring, 35 mL of aniline monomer was added to the dispersion, followed by 1.335 mmol of PA as the dopant. The reaction was left to take place at room temperature for 6 h. To obtain the PA-PANI material, the resulting product was collected by high-speed centrifugation, washed thoroughly with deionized water and ethanol, and dried under vacuum at 60 °C for 24 h. PA-PANI samples with various PA molar ratios were prepared similarly to determine the effect of PA content on the adsorption performance. Figure 1 shows the synthesis pathway of PA-PANI.

Synthesis of CS/PA-PANI

A total of 100.0 mg of PA-PANI was suspended in 10.0 mL of deionized water. Separately, 0.15 g chitosan powder was dissolved in 10.0 mL 2% acetic acid solution, and the dissolved chitosan solution was added dropwise to the PA-PANI dispersion. The mixture was stirred for 12 h. The product (CS/PA-PANI) was then collected, washed thoroughly with deionized water, and dried under vacuum at 60 °C for 24 h. The mass increase was used to determine the chitosan loading on PA-PANI using the following equation:

$$\text{Loading amount } (\%) = \frac{W_m - W_0}{W_0} \times 100\% \quad (1)$$

where, W_0 and W_m are the weights of the material before and after chitosan loading, respectively.

Synthesis of HCl-PANI

For comparison, the hydrochloric acid-doped polyaniline CS/HCl-PANI was also prepared by replacing the PA aqueous solution with 1 mol L^{-1} of hydrochloric acid solution.

Uranium is extracted electrochemically

The CDI system was constructed using acrylic plates with titanium (Ti) sheets as current collectors and 1-mm-thick silicone gaskets to separate the anode and cathode chambers. The electrodes were prepared by simply mixing the active material (CS/PA-PANI or PA-PANI), Ketjen Black (conductive additive), and polyvinylidene fluoride (PVDF) binder in a mass ratio of 8:1:1. CDI electrodes were obtained by dispersing the mixture in N-methyl-2-pyrrolidone (NMP) and spray-coated it onto Ti sheets (40 × 40 mm), followed by drying at 60 °C over a period of 12 h. During the operation of CDI, the prepared materials (CS/PA-PANI or PA-PANI), and commercial AC were used as cathode and anode, respectively. The adsorption performance was evaluated under various operating conditions, such as applied voltage (0–1.2 V), solution pH (3–9), and initial U(VI) concentration. Ultraviolet-visible spectrophotometry (UV-6000, Shanghai Tongwei Analysis Technology Co., Ltd, China) and inductively coupled plasma mass spectrometry (ICP-MS; Agilent 7850, USA) were used to measure the concentrations of uranyl ions before and after adsorption. Detailed instrument parameters, physical-chemical adsorption experimental procedures, and electrochemical test conditions can be found in the Supplementary Experiment.

Calculations of extraction capacity

The equilibrium uranium extraction capacity (q_e, mg g^{-1}), the uranium extraction capacity at time t (q_t, mg g^{-1}), and the removal efficiency of the uranyl ions (RE%) was determined by the following equations:

$$q_e = \frac{(C_i - C_e) \times V}{W} \quad (2)$$

$$q_t = \frac{(C_i - C_t) \times V}{W} \quad (3)$$

$$RE\ (\%) = \frac{(C_i - C_e)}{C_i} \times 100\% \quad (4)$$

where, C_i and C_e represent the starting concentration and equilibrium concentration of uranium ions (mg L^{-1}), respectively, V (mL) is the abbreviation of volume of the solution, and W is the mass of adsorbent (mg).

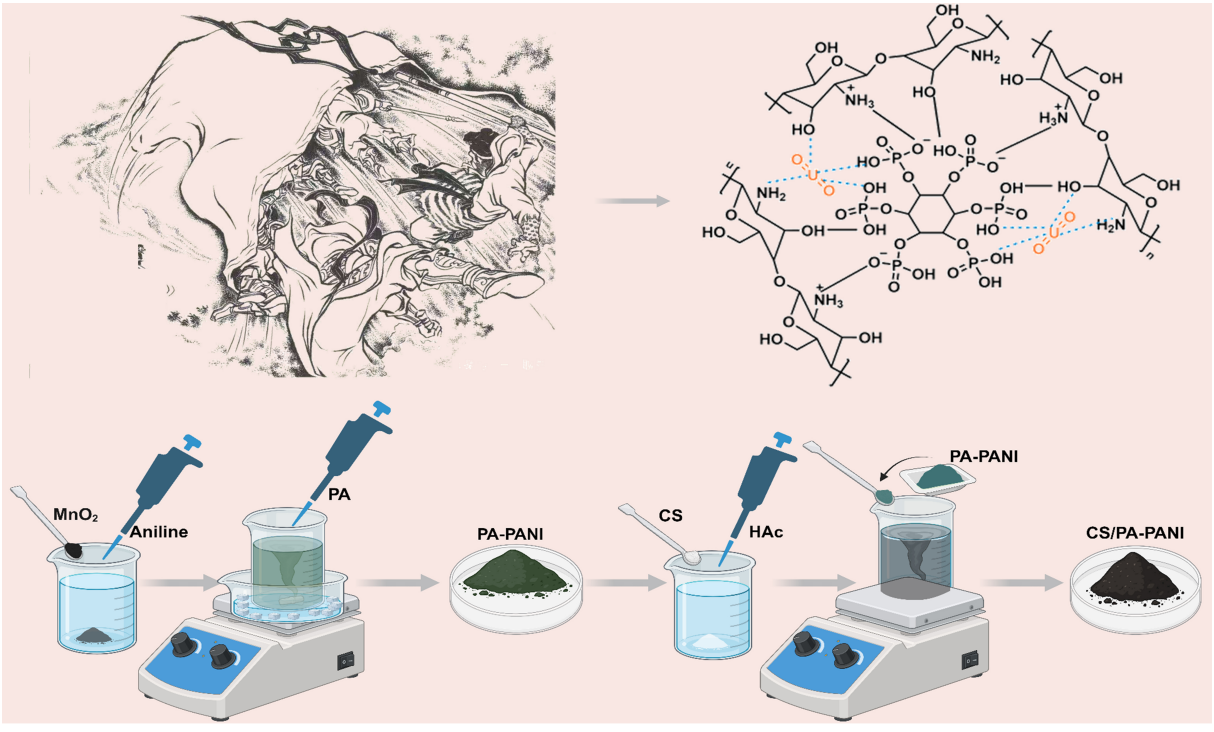

Fig. 1 The preparation process of CS/PA-PANI.

https://doi.org/10.48130/scm-0026-0011

Reuse of CS/PA-PANI electrodes

To evaluate the cyclic electrochemical extraction performance of CS/PA-PANI, the electrode used in a 200 mg L^{-1} uranyl solution, was regenerated by applying a reverse voltage in 0.1 mol L^{-1} HCl for 4 h. This adsorption-desorption process was repeated five times, and the extraction capacity was calculated for each cycle. In a parallel experiment, the spent electrode was immersed in 50 mL of a 100 mg L^{-1} uranyl solution for 24 h to assess physical-chemical adsorption. The used electrode was then eluted in 0.1 mol L^{-1} of HNO_3 for 8 h.

Results and discussion

The potential of conducting polymers like polyaniline (PANI) to bind uranyl ions forms the basis for synthesizing efficient uranium adsorption materials. To enhance the selective binding and conversion of the uranyl ions, PA—a molecule with high coordination affinity for U(VI)—was used as a dopant to PANI, and chitosan was subsequently added to the surface to further increase selectivity and adsorption capacity. SEM images of CS/PA-PANI (Fig. 2a, b) showed a spherical morphology of the compound, which is advantageous for increasing surface area and adsorption capacity. Elemental mapping (Supplementary Fig. S1) confirmed the presence of C, N, O, and P as expected. The FTIR spectra showed characteristic peaks of PA-PANI at 1,133, 1,053, and 505 cm^{-1} corresponding to P–O, P–O–P, and PO_4^{3-} groups, respectively[45,46]. The prominent peak at 1,615 cm^{-1} was attributed to the stretching vibration of the ring of quinone-like structures, confirming the successful introduction of phytate into the PANI structure. Following the assembly of chitosan, the typical –OH and $–NH_2$ stretching bands at 3,200–3,500 cm^{-1} were observed to be significantly intensified and shifted, indicating that CS was bonded to PA-PANI via electrostatic interactions and hydrogen bonding[47,48] (Fig. 2c). The presence of C, O, N, and P was further confirmed by X-ray photoelectron spectroscopy (Fig. 2d). The intensities of –OH and P–O–C peaks in CS/PA-PANI were significantly higher in the high-resolution O 1s spectrum (Fig. 2e), and the area ratio of P–O–C/P=O increased with the ratio shifting to 2.02 in the CS/PA-PANI (compared to 0.97 for PA-PANI). This pronounced change provided strong evidence for successful chitosan grafting. Thermogravimetric analysis (TGA) was performed to evaluate the thermal stability; both PA-PANI and CS/PA-PANI showed comparable degradation behavior, beginning at approximately 200 °C (Fig. 2f). Reduced carbon content following CS recombination by a slight

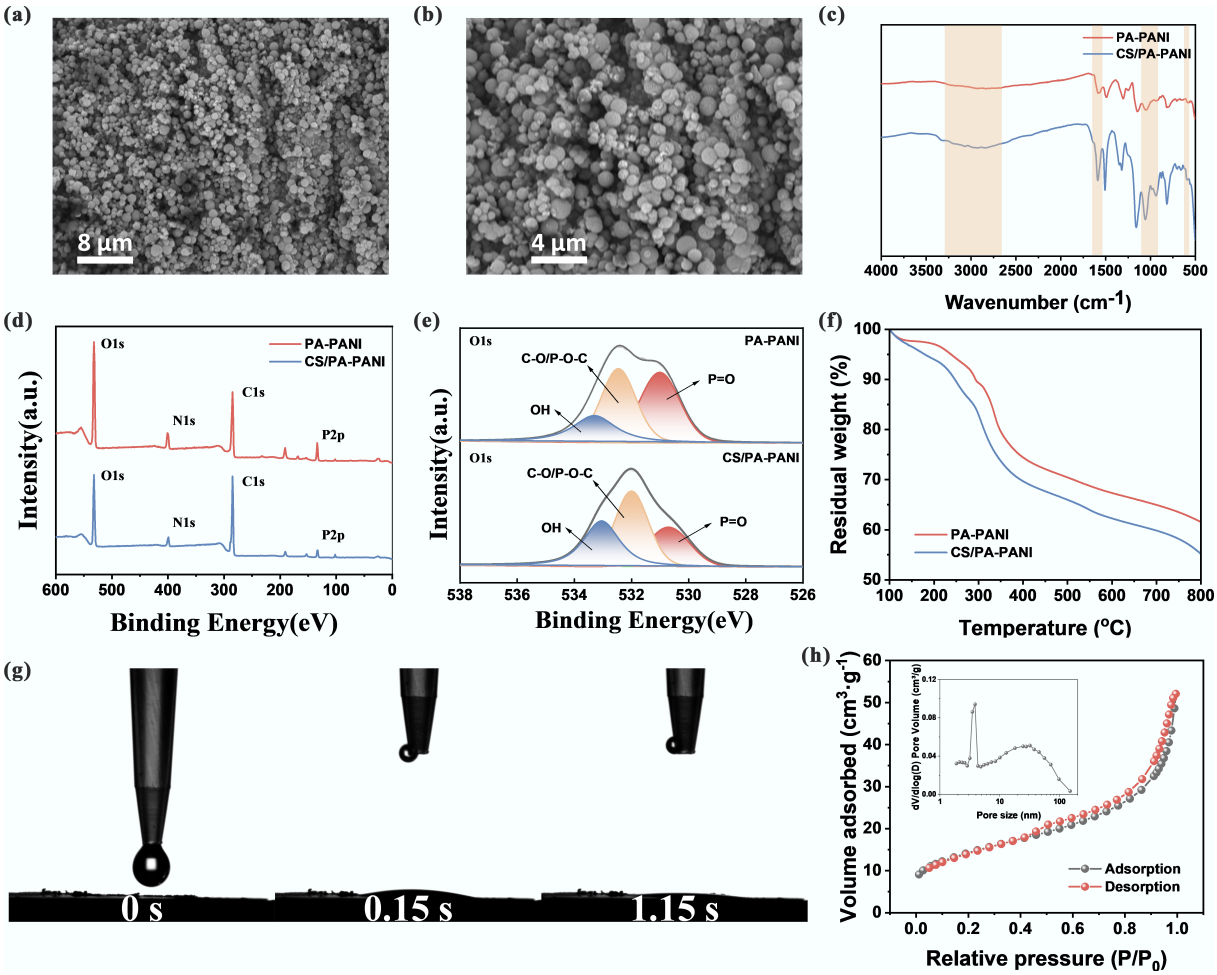

Fig. 2 Synthesis and characterization of CS/PA-PANI. (**a**), (**b**) SEM of CS/PA-PANI. (**c**) FTIR of PA-PANI and CS/PA-PANI; (**d**) XPS survey spectroscopy of PA-PANI and CS/PA-PANI; (**e**) XPS O 1s spectra deconvoluted to components at high resolution; (**f**) Thermogravimetric analysis (TGA) profiles in N_2 atmosphere; (**g**) Time dependent evolution of water contact angle and hysteresis of CS/PA-PANI; (**h**) N_2 adsorption-desorption curve and corresponding pore size distribution (inset) of CS/PA-PANI.

margin was in line with TGA findings. Hydrophilicity, which is crucial for adsorption kinetics was assessed by measuring the contact angle at rest. CS/PA-PANI showed rapid water droplet absorption, with complete wetting occurring within about 1.15 s, indicating excellent wettability (Fig. 2g). This hydrophilicity promotes mass transfer to a large extent, thereby enhancing adsorption efficiency. As shown in Fig. 2h, CS/PA-PANI exhibited a microporous and mesoporous structure with an average pore diameter of 45.2 nm and a large specific surface area, which contributed to enhanced charge storage[49]. These architectural benefits provided vast channels of ion transport and active sites, enabling effective adsorption of the U(VI) in the subsequent CDI applications.

Figure 3a shows that the cyclic voltammetry (CV) of the CS/PA-PANI electrode exhibited a progressive increase in integrated area at scan rates ranging from 10 to 100 mV s^{-1}[50]. Figure 3b shows that the specific capacitance of the CS/PA-PANI electrode decreased with the reduction of the scan rate, which could be attributed to the diffusion and migration of uranyl ions to the electroactive sites, limiting the charge storage capacity at high scan rates[51]. Electrochemical impedance spectroscopy (EIS) was also used to evaluate the conductivity and charge-transfer properties of CS/PA-PANI and PA-PANI electrodes (Fig. 3c)[52]. Calculations indicated that the ionic conductivity of CS/PA-PANI reached 189.04 S cm^{-1}. All results support the view that the CS/PA-PANI electrode served as an efficient electroadsorbent for uranyl ions, demonstrating outstanding electrochemical performance and broad application potential.

To evaluate the electrosorption capacity of CS/PA-PANI for hexavalent uranium, batch adsorption experiments were conducted in the self-assembled CDI system depicted in Fig. 4a. The electrode featured an effective area of 16 cm^2 with a parallel-plate structure, maintaining a precisely controlled inter-electrode gap of 2 mm. The electrolyte consisted of 50 mL uranium nitrate solution, circulated at a constant flow rate of 20 mL min^{-1} via a peristaltic pump to ensure the system maintained a controlled laminar flow state (Reynolds number Re < 100). The influence of concentration of the PA dopant on the uranyl ion extraction was methodically investigated (Fig. 4b). As shown in Supplementary Fig. S2, the mass fraction of phosphorus in PA-PANI increased continuously with the rising PA doping ratio, indicating a progressive increase in PA incorporation. The findings showed that the uranium adsorption capacity was proportional to the PA content at lower ratios of doping. An optimal monomer-to-PA molar ratio of 10:2.5 yielded the highest extraction capacity of 823.7 mg g^{-1}. Remarkably, the uranium uptake decreased considerably at a higher doping ratio of 1:0.3, to 762.3 mg g^{-1}, which may be explained by the nature of intrinsic impedance of the PA-PANI composite. Although increased levels of PA provided more phosphate binding sites, the material with a monomer-to-PA molar ratio of 1:0.2 exhibited superior charge transport characteristics, thus providing the ability to capture uranyl ions more effectively. The loading of chitosan on the PA-PANI surface (Fig. 4c) increased at a high rate in the early stages and then became stagnant with prolonged reaction time. It is important to note that at a critical chitosan loading of approximately 29%, the adsorption performance of the CS/PA-PANI composite was maximized. The additional increase of the loading time after 8 h, however, resulted in the adsorption being reduced by approximately 9% (Fig. 4d). It is assumed that this non-monotonic tendency was caused by the rearrangement of the structure caused by excess chitosan: on the one hand, excessive chitosan molecules may block the mesoporous channels of PA-PANI; on the other hand, the long-duration reaction could disrupt the PANI backbone. Compared to the individual components, CS/PA-PANI exhibited significantly superior adsorption performance (Fig. 4e). As solution pH and applied voltage have been determined to be critical factors affecting UO_2^{2+} adsorption, electrosorption activity of CS/PA-PANI was further investigated regarding various pH conditions (3–9), and applied voltage (0–1.2 V). The pH influence on the adsorption performance is shown in Fig. 4f. The adsorption capacity of CS/PA-PANI initially increased and then decreased with increasing pH, and the highest adsorption capacity was achieved at pH 5. According to previous works, UO_2^{2+} is the dominant species of a solution with pH values below 5. Under low pH conditions, the high content of H^+ ions causes the adsorbent surface to be protonated, causing electrostatic repulsion with UO_2^{2+}, and decreasing the adsorption capacity. With increasing pH, the negatively charged uranium species such as $UO_2(OH)_3^-$ and $(UO_2)_3(OH)_7^-$ become dominant and consequently, negatively charged adsorbent surface starts to be repelled, and adsorption efficiency is further reduced[53]. Thus, all the experiments were performed at pH 5 unless otherwise specified. Moreover, the operation of electrosorption of CS/PA-PANI with U(VI) was highly dependent on the voltage applied. Under the open-circuit conditions, the adsorption capacity was fairly low at 599.4 mg g^{-1}. Nevertheless, the adsorption capacity increased with the voltage applied, with an increase in the adsorption capacity of U(VI) from 599.4 to 942.4 mg g^{-1} at 0 and 1.2 V, respectively, as the driving force, the electric force increased in strength and enhanced the rate of uptake of U(VI) (Fig. 4g). Given the fact that too high voltages can cause Faradaic reactions like the electrolysis of water (1.23 V vs SHE), and

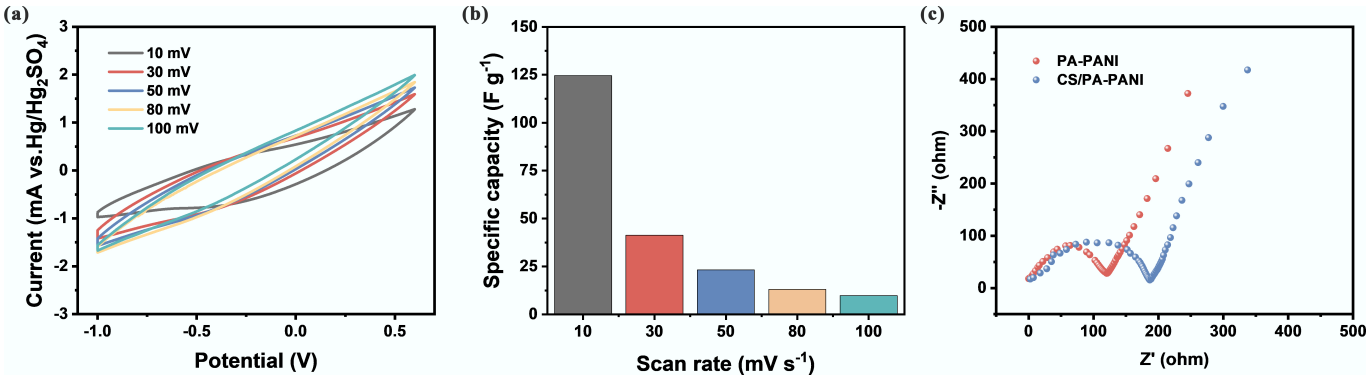

Fig. 3 Electrochemical performance evaluation of CS/PA-PANI. (**a**) CV curves of CS/PA-PANI at various scanning rates; (**b**) Specific capacitance of CS/PA-PANI at various scanning rates; (**c**) EIS spectra of the CS/PA-PANI and PA-PANI.

https://doi.org/10.48130/scm-0026-0011

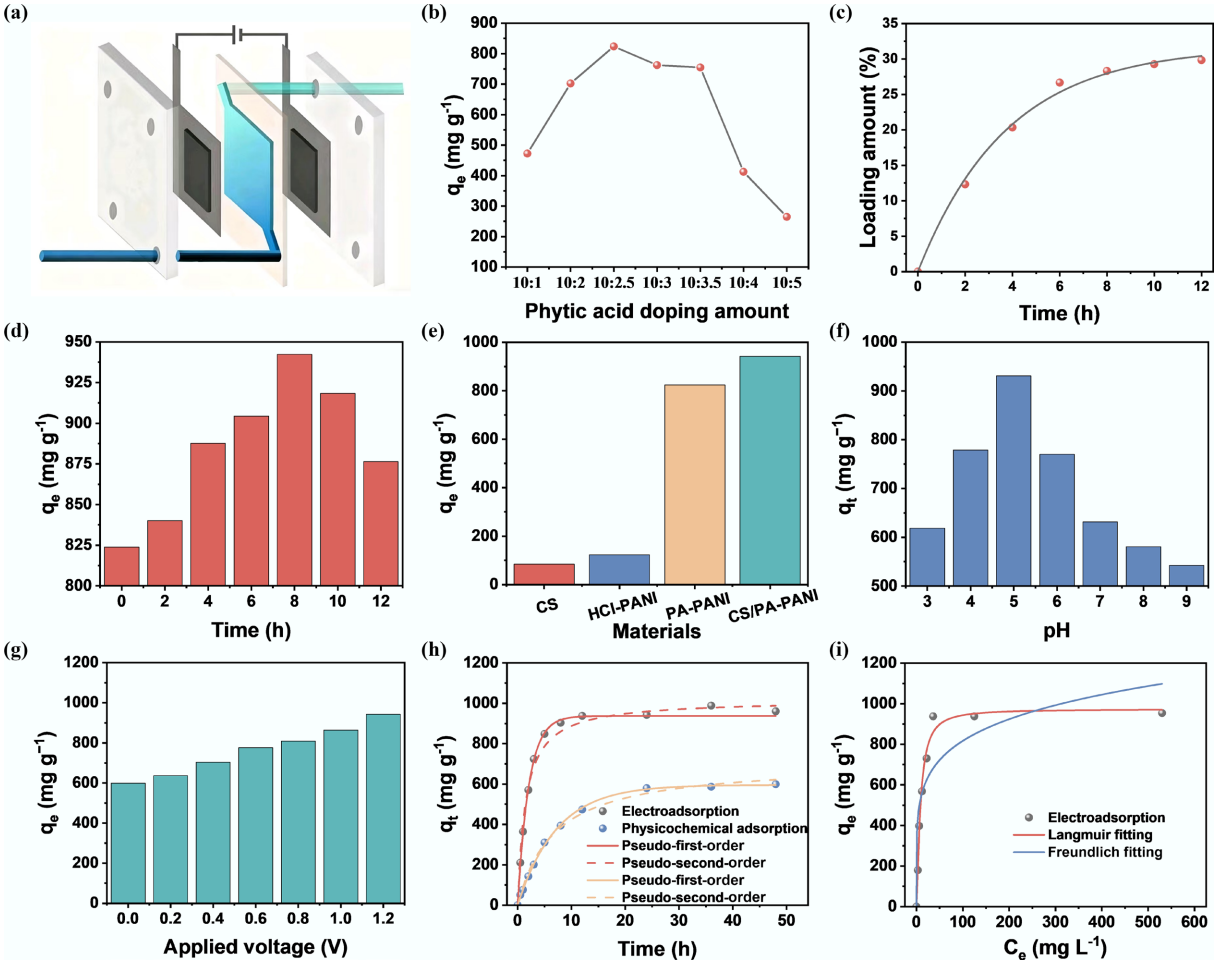

Fig. 4 Uranium electrosorption behavior of CS/PA-PANI electrodes. (**a**) Schematic illustration of CS/PA-PANI employed as an immobile electrode in the CDI system. (**b**) Effect of phytic acid doping amount on uranium electrosorption. (**c**) Change of chitosan loading concentration with time. (**d**) Effect of chitosan doping time on adsorption performance. (**e**) U(VI) electrosorbed by various samples. Influence of pH of (**f**) solution and voltage (**g**) applied on U(VI) electrosorption. (**h**) Kinetics of adsorption CS/PA-PANI with the respective fitting equations in the model of pseudo-first-order and pseudo-second-order. (**i**) Adsorption isotherms at initial U(VI) concentrations of 50, 100, 200, 300, 400, and 500 mg L^{-1}. Experimental conditions: solution volume: 50 mL; pH adjusted using dilute Na_2CO_3 or HNO_3 solution.

will result in inefficiency in energy conversion, 1.2 V was selected as the standard voltage for the subsequent experiments. Figure 4h shows the adsorption kinetics of CS/PA-PANI under open-circuit and 1.2 V conditions. In comparison with physical and chemical adsorption, electrosorption reached equilibrium more rapidly, typically within 12 h. The corresponding equilibrium adsorption capacities were 942.4 mg g^{-1} for electrosorption, and 599.4 mg g^{-1} for physical-chemical adsorption. The adsorption kinetics data were further analyzed using pseudo-first-order and pseudo-second-order models[54,55]. For electrosorption and physical-chemical adsorption, the correlation coefficients (R^2) of the pseudo-first-order model were 0.9736 and 0.9910, respectively (Supplementary Table S1), and the values of R^2 in the pseudo-second-order model were 0.9896 and 0.9947. The higher R^2 values confirmed that the pseudo-second-order model better described the electrosorption process, indicating that this process was dominated by surface redox reactions and capacitive energy storage mechanisms. The adsorption isotherms play a vital role in the characterization of adsorption of materials. Electrosorption was carried out on CS/PA-PANI using uranium solutions of different concentrations. The Langmuir model (R^2 = 0.9817) provided an excellent fit to the experimental equilibrium data, as shown in Fig. 4i. The calculated maximum adsorption capacity of 973.1 mg g^{-1} at an initial uranium concentration of 600 mg L^{-1} was well in agreement with the experimental value of 954.1 mg g^{-1} (Supplementary Table S2).

Electrode reusability is a major consideration for practical applications. The cycling stability of the CS/PA-PANI electrode was tested by applying a reverse bias to the electrode within 4 h, eluting with 0.1 mol L^{-1} of HCl. As shown in Fig. 5a, after five cycles in a 50 mL solution containing 200 mg L^{-1} of uranyl acetate, the extraction capacity and removal efficiency decreased to 314.5 mg^{-1} and 78%, respectively. This reduction can probably be attributed to the desorption or loss of the PA and chitosan molecules during the electrodeposition process. Although the extraction capacity decreased with cycle number, the high inherent binding of CS/PA-PANI to uranyl ions enabled the spent electrodes to be further utilized via physical-chemical adsorption to maximize the use of adsorption sites. Five consecutive adsorption cycles with 50 mL 100 mg L^{-1} uranyl solution were conducted using the spent electrodes, and the removal efficiency of the electrode decreased to 74%. This combined approach of electrochemical deposition and physical-chemical adsorption allows full utilization of the electrode capacity,

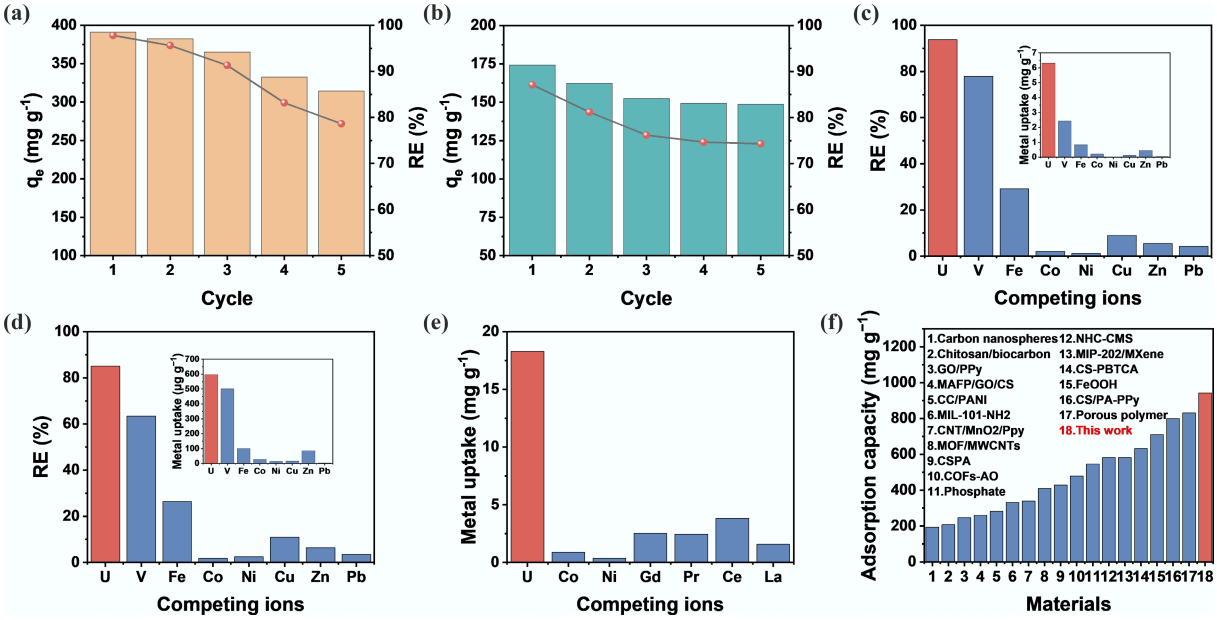

Fig. 5 Cycling stability and selectivity of CS/PA-PANI electrodes in uranium recovery. (**a**) Cycling reversibility of CS/PA-PANI electrodes eluted with 0.1 mol L^{-1} HCl under reverse bias for 4 h. The starting concentration, C_0 = 200 mg L^{-1}. (**b**) Five adsorption cycles and one elution of used CS/PA-PANI electrodes with 0.1 mol L^{-1} HNO_3 as the eluent. C_0 = 100 mg L^{-1}. (**c**) Uranium and competing ion uptake by CS/PA-PANI into U-spiked simulated seawater. (**d**) Comparison of adsorption of uranium in the natural seawater with other competing ions. (**e**) Co-removal of a mixture of ions on the CS/PA-PANI electrode through simulated nuclear wastewater after 24 h. (**f**) Comparison of the uranium adsorption capacity of CS/PA-PANI with reported adsorbents[26, 32,33, 50,56–67].

which is important for environmental sustainability and cost-effective industrial application. Different competing ions in the seawater may influence the uranium adsorption capacity of the adsorbent. Uranium adsorption behavior of CS/PA-PANI was tested in simulated seawater (Supplementary Table S3) and natural seawater (Supplementary Table S4), which is similar to open-sea conditions. As shown in Fig. 5c, among competing ions, the CS/PA-PANI composite exhibited the highest adsorption capacity for uranium, with a U/V ratio of 2.6, and a U/Fe ratio of 7.5. The selectivity coefficients for other interfering ions all exceeded 10. To evaluate its performance in natural seawater, long-term continuous adsorption experiments were also conducted. Figure 5d indicates that after 10 d, the uranium removal rate reached 85%, the U/V ratio decreased to 1.2, and the U/Fe ratio decreased to 6.0, while the selectivity coefficients for other interfering ions remained above 7. This variation reflects the impact of the complex ionic environment in real seawater on separation efficiency. Uranium extraction experiments were also conducted in the model radioactive nuclear wastewater to investigate the increased applicability of CS/PA-PANI electrodes. U(VI), Ni(II), Co(II), Gd(III), Pr(III), Ce(III), and La(III) were present in the prepared solution at a concentration of 0.05 mmol L^{-1}. Figure 5e shows that after 24 h, CS/PA-PANI attained a uranium extraction capacity of 18.3 mg g^{-1}, which was several times greater than that of the other competitive ions, indicating the electrode's efficacy for uranium removal from radioactive nuclear wastewater. The performance of CS/PA-PANI in removing uranium was again compared with the performance of various reported CDI electrode materials (Fig. 5f and Supplementary Table S5), and CS/PA-PANI showed the best performance among the reported electrodes. Additionally, the energy consumption per unit of uranium removed during the electrosorption process was calculated to be 3.81 Wh kg^{-1}, indicating extremely low electrical energy consumption. These values provide key reference metrics for evaluating the efficiency and practicality of electrodes in uranium recovery from aqueous solutions, highlighting their application potential in low-energy-consumption, high-performance electrosorption systems.

XPS analysis (Fig. 6a) revealed specific peaks for C 1s, O 1s, N 1s, P 2p, and U 4f. The appearance of the U 4f peak confirms the successful adsorption of U onto CS/PA-PANI, which proves its capability to adsorb U in aqueous solutions. To elucidate the adsorption mechanism of UO_2^{2+} on CS/PA-PANI, high-resolution XPS O 1s and N 1s spectra were deconvoluted before and after adsorption (Supplementary Fig. S3). In the post-adsorption O 1s spectrum, a new fitted peak appeared at higher binding energy, attributed to U–O bonds formed via UO_2^{2+} coordination. Concurrently, peaks associated with phosphate groups from PA and hydroxyl groups from CS exhibited shifts, indicating their direct involvement in uranium binding. The N 1s spectrum further revealed a shift of the amine peak to higher binding energy, confirming the chelation of UO_2^{2+} by nitrogenous functional groups. These findings demonstrate that both oxygen-rich (PO_4^{3-}, –OH) and nitrogen-rich ($–NH_2$) sites in CS/PA-PANI actively participate in uranium removal, validating a synergistic mechanism where electrosorption (capacitive), and physicochemical adsorption (chelation) jointly govern UO_2^{2+} uptake. Furthermore, the coordination modes between the functional groups on CS/PA-PANI and uranyl ions were also investigated based on density functional theory (DFT) calculations (Fig. 6b). Single-point energy calculations showed that the adsorption energy between the functional groups and UO_2^{2+} was −22.40 eV, indicating that the functional groups had a strong affinity to uranyl ions. ESP mapping reveals that the ESP of UO_2^{2+} overlaps with that of the functional groups (Fig. 6c), providing further evidence for the interaction between UO_2^{2+} and the polyaniline-based functional groups. The

https://doi.org/10.48130/scm-0026-0011

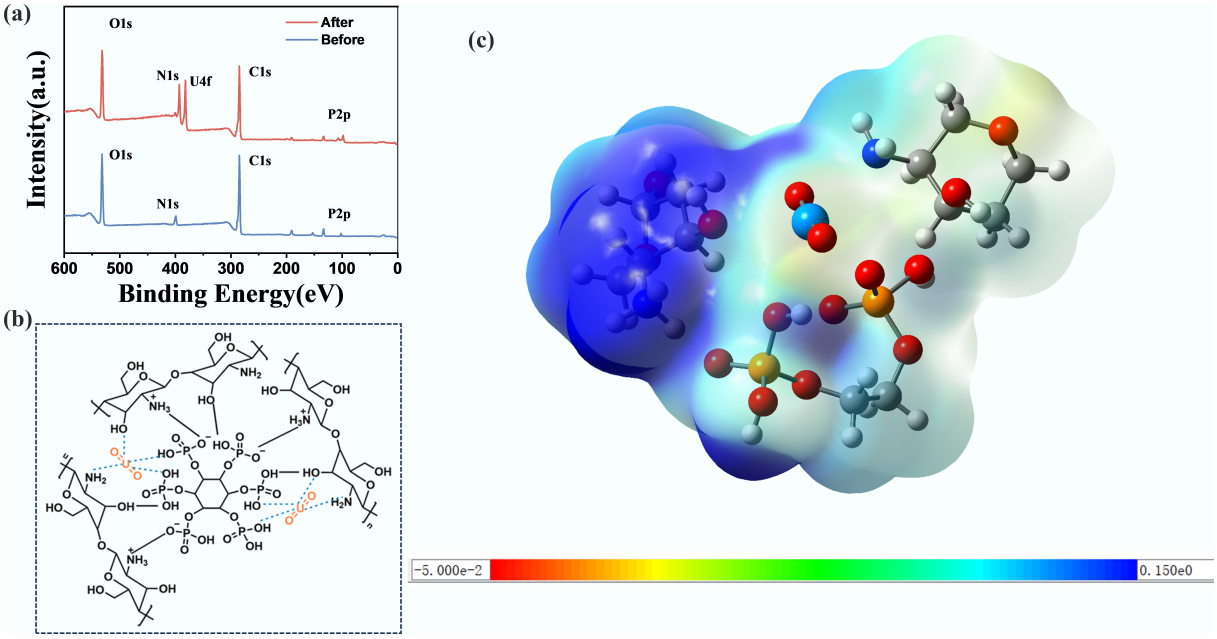

Fig. 6 Mechanistic study of uranium adsorption by CS/PA-PANI composites. (**a**) XPS spectra of the CS/PA-PANI before and after U adsorption. (**b**) Structural schematics of functional groups in CS/PA-PANI. (**c**) Coordination structure diagram of functional groups in CS/PA-PANI with uranyl ion.

high adsorption capacity of CS/PA-PANI renders it a potential use in the large-scale extraction of uranium from seawater and recovery from nuclear wastewater. Its low-cost material composition is advantageous for large-scale industries. The excellent uranium adsorption capacity enhances extraction efficiency, while the good recovery of uranium guarantees long-term stability of electrodes. These properties collectively make CS/PA-PANI an efficient, cost-effective, durable, and scalable material for uranium extraction.

Conclusions

In this study, we successfully synthesized a novel, cost-effective CS/PA-PANI, with both electrochemical and physicochemical adsorption capabilities. CS/PA-PANI was synthesized via a simple and generalized heterogeneous polymerization technique and has inherent conductivity. The functional groups of PA and CS render the molecules hydrophilic and a high binding affinity for uranyl ions, enabling phosphate and hydroxyl groups to interact with UO_2^{2+}. The maximum adsorption capacity of the CS/PA-PANI electrode under an applied voltage of 1.2 V was a saturation adsorption capacity of 942.4 mg g^{-1}, compared to the physical-chemical adsorption capacity of 599.4 mg g^{-1}. After 10 d of physical-chemical adsorption in 3 L of natural seawater, the uranium concentration dropped to 0.4 ug L^{-1}, compared with an initial concentration of 2.4 ug L^{-1}. Recycling of spent electrodes enables the maximum utilization of electrodes in terms of cost and performance. On the whole, this environmentally friendly, energy-saving and efficient strategy holds significant potential for large-scale industries application. Furthermore, the production of the CS/PA-PANI electrodes offers insights into the application of functionalized conductive polymers for the extraction and reuse of ions.

Supplementary information

It accompanies this paper at: https://doi.org/10.48130/scm-0026-0011.

Author contributions

The authors confirm their contributions to the paper as follows: Chenxiao Hong: original draft, visualization, validation, methodology, investigation, formal analysis, data curation. Jing Wang: original draft, visualization, validation, methodology, investigation, formal analysis, data curation. Sana Shafia: visualization, methodology, formal analysis, data curation. Jiayao Hu: methodology, investigation. Junyi Chen: methodology, investigation. Ilhom Halimov: writing – review and editing, supervision, project administration. Jiaxing Li: resources, visualization, supervision, software, project administration, funding acquisition, formal analysis, conceptualization, writing – review and editing. All authors reviewed the results and approved the final version of the manuscript.

Data availability

The datasets generated during and/or analyzed during the current study are available from the corresponding author on reasonable request.

Acknowledgments

The authors give credit to National Natural Science Foundation of China and the financial support given by the Priority Academic Program Development of Jiangsu Higher Education Institutions are acknowledged. We also thank Ilhom Halimov's group from Navoi State University of Mining and Technologies for their support.

Funding

This paper was sponsored by the National Natural Science Foundation of China (22276195).

Declarations

Competing interests

The authors have not mentioned any conflict of interest.

Author details

[1]Science Island Branch, University of Science and Technology of China, Hefei 230026, China; [2]Institute of Plasma Physics, Hefei Institutes of Physical Science, Chinese Academy of Sciences, Hefei 230031, China; [3]Navoi State University of Mining and Technologies, Navoi 210100, Uzbekistan

References

[1] Hoffert MI, Caldeira K, Benford G, Criswell DR, Green C, et al. 2002. Advanced technology paths to global climate stability: energy for a greenhouse planet. *science* 298:981−987

[2] Chu S, Majumdar A. 2012. Opportunities and challenges for a sustainable energy future. *Nature* 488:294−303

[3] Adamantiades A, Kessides I. 2009. Nuclear power for sustainable development: current status and future prospects. *Energy Policy* 37:5149−5166

[4] Degueldre C, Bertsch J, Kuri G, Martin M. 2011. Nuclear fuel in generation II and III reactors: research issues related to high burn-up. *Energy & Environmental Science* 4:1651−1661

[5] Mayer K, Wallenius M, Lützenkirchen K, Horta J, Nicholl A, et al. 2015. Uranium from german nuclear power projects of the 1940s – a nuclear forensic investigation. *Angewandte Chemie International Edition* 54:13452−13456

[6] Abney CW, Mayes RT, Saito T, Dai S. 2017. Materials for the recovery of uranium from seawater. *Chemical Reviews* 117:13935−14013

[7] Sholl DS, Lively RP. 2016. Seven chemical separations to change the world. *Nature* 532:435−437

[8] Lindner H, Schneider E. 2015. Review of cost estimates for uranium recovery from seawater. *Energy Economics* 49:9−22

[9] Kim J, Tsouris C, Mayes RT, Oyola Y, Saito T, et al. 2013. Recovery of uranium from seawater: a review of current status and future research needs. *Separation Science and Technology* 48:367−387

[10] Wang C, Helal AS, Wang Z, Zhou J, Yao X, et al. 2021. Uranium *in situ* electrolytic deposition with a reusable functional graphene-foam electrode. *Advanced Materials* 33:2102633

[11] Manos MJ, Kanatzidis MG. 2012. Layered metal sulfides capture uranium from seawater. *Journal of the American Chemical Society* 134:16441−16446

[12] Zhao S, Yuan Y, Yu Q, Niu B, Liao J, et al. 2019. A dual-surface amidoximated halloysite nanotube for high-efficiency economical uranium extraction from seawater. *Angewandte Chemie International Edition* 58(42):14979−14985

[13] Kou S, Yang Z, Sun F. 2017. Protein hydrogel microbeads for selective uranium mining from seawater. *ACS Applied Materials & Interfaces* 9:2035−2039

[14] Yu Q, Yuan Y, Feng L, Feng T, Sun W, et al. 2020. Spidroin-inspired, high-strength, loofah-shaped protein fiber for capturing uranium from seawater. *Angewandte Chemie International Edition* 59:15997−16001

[15] Katsoyiannis IA, Althoff HW, Bartel H, Jekel M. 2006. The effect of groundwater composition on uranium(VI) sorption onto bacteriogenic iron oxides. *Water Research* 40:3646−3452

[16] Barton CS, Stewart DI, Morris K, Bryant DE. 2004. Performance of three resin-based materials for treating uranium-contaminated groundwater within a PRB. *Journal of Hazardous Materials* 116:191−204

[17] Sorg TJ. 1988. Methods for removing uranium from drinking water. *Journal-American Water Works Association* 80:105−111

[18] Shen J, Schäfer A. 2014. Removal of fluoride and uranium by nanofiltration and reverse osmosis: a review. *Chemosphere* 117:679−691

[19] Huang J, Liu Z, Huang D, Jin T, Qian Y. 2022. Electrochemical deposition of uranium oxide with an electrocatalytically active electrode using double potential step technique. *Chinese Chemical Letters* 33:3762−3766

[20] Liu Y, Tian R, Zhang S, Bo T, Wang Z, et al. 2024. Capacitive deionization of uranium mediated by dioxygen functionalities in the C=O=C=O segment of polyacrylic acid-functionalized graphene aerogel. *Chemical Engineering Journal* 481:148388

[21] Shi N, Wu J, Zhi X, Li N, Wang Z. 2023. Amidoxime-functionalized cellulose nanofibers/MXene aerogel for electric field enhanced uranium extraction from seawater. *Chemical Engineering Journal* 476:146563

[22] Huang J, Liu Z, Huang D, Jin T, Qian Y. 2022. Efficient removal of uranium(VI) with a phytic acid-doped polypyrrole/carbon felt electrode using double potential step technique. *Journal of Hazardous Materials* 433:128775

[23] Liao Y, Wang M, Chen D. 2019. Electrosorption of uranium(VI) by highly porous phosphate-functionalized graphene hydrogel. *Applied Surface Science* 484:83−96

[24] Zhou J, Zhang X, Zhang Y, Wang D, Zhou H, et al. 2022. Effective inspissation of uranium(VI) from radioactive wastewater using flow electrode capacitive deionization. *Separation and Purification Technology* 283:120172

[25] Yan B, Ma C, Gao J, Yuan Y, Wang N. 2020. An ion-crosslinked supramolecular hydrogel for ultrahigh and fast uranium recovery from seawater. *Advanced Materials* 32:1906615

[26] Tauk M, Bechelany M, Sistat P, Habchi R, Cretin M, et al. 2024. Ion-selectivity advancements in capacitive deionization: a comprehensive review. *Desalination* 572:117146

[27] Zhang J, Wang Y, Wei Y, Xu M, Hu Y, et al. 2024. Magnetic CNT-based electrode for efficient electro-adsorption of uranium. *Journal of Environmental Chemical Engineering* 12:112160

[28] Liao Y, Lei R, Weng X, Yan C, Fu J, et al. 2023. Uranium capture by a layered 2D/2D niobium phosphate/holey graphene architecture via an electro-adsorption and electrocatalytic reduction coupling process. *Journal of Hazardous Materials* 442:130054

[29] Ali Ansari S, Parveen N, Ansari MZ, Alsulaim GM, Alam MW, et al. 2025. Exploring recent advances in the versatility and efficiency of carbon materials for next generation supercapacitor applications: a comprehensive review. *Progress in Materials Science* 154:101493

[30] Parveen N. 2025. Enhanced energy storage using bio-waste derived carbon and three-dimensional $NiCo_2O_4$ structures in asymmetric supercapacitors. *Journal of Industrial and Engineering Chemistry* 150:824−836

[31] Lakard S, Lakard B. 2025. Environmental applications of conducting polymers and their composites: adsorption and detection of heavy metal ions. *Journal of Environmental Chemical Engineering* 13:116233

[32] Yu H, Zhou L, Liu Y, Ao X, Ouyang J, et al. 2023. Biocarbon/polyaniline nanofiber electrodes with high hybrid capacitance and hierarchical porous structure for U(VI) electrosorption. *Desalination* 564:116773

[33] Shuang M, Zhou L, Liu Y, Yu H, Ao X, et al. 2023. Electrodeposition nanofabrication of graphene oxide/polypyrrole electrodes with high hybrid specific capacitance for enhancing U(VI) electrosorption. *Journal of Environmental Chemical Engineering* 11:111498

[34] Chen D, Wu W, Zhao X, Feng D, Zhao R, et al. 2023. Continuous polypyrrole nanotubes encapsulated Co_3O_4 nanoparticles with oxygen vacancies and electron transport channels boosting peroxymonosulfate activation. *Nano Research* 16:11018−11029

[35] Nezakati T, Seifalian A, Tan A, Seifalian AM. 2018. Conductive polymers: opportunities and challenges in biomedical applications. *Chemical Reviews* 118:6766−6843

[36] Hodgson AJ, Gilmore K, Small C, Wallace GG, MacKenzie IL, et al. 1994. Reactive supramolecular assemblies of mucopolysaccharide, polypyrrole and protein as controllable biocomposites for a new generation of 'intelligent biomaterials'. *Supramolecular Science* 1:77−83

[37] Kargirwar SR, Thakare SR, Choudhary MD, Kondawar SB, Dhakate SR. 2011. Morphology and electrical conductivity of self-doping polyanilines synthesized via self-assembly process. *Advanced Materials Letters* 2:397−401

[38] Zou Y, Chen Z, Guo X, Peng Z, Yu C, et al. 2022. Mechanically robust and elastic graphene/aramid nanofiber/polyaniline nanotube

aerogels for pressure sensors. *ACS Applied Materials & Interfaces* 14:17858–17868
[39] Wang X, Zhang D, Zhang H, Gong L, Yang Y, et al. 2021. *In situ* polymerized polyaniline/MXene (V2C) as building blocks of supercapacitor and ammonia sensor self-powered by electromagnetic-triboelectric hybrid generator. *Nano Energy* 88:106242
[40] Yu P, Zhang Z, Zheng L, Teng F, Hu L, et al. 2016. A novel sustainable flour derived hierarchical nitrogen-doped porous carbon/polyaniline electrode for advanced asymmetric supercapacitors. *Advanced Energy Materials* 6:1601111
[41] Song E, Choi JW. 2013. Conducting polyaniline nanowire and its applications in chemiresistive sensing. *Nanomaterials* 3:498–523
[42] Baker CO, Huang X, Nelson W, Kaner RB. 2017. Polyaniline nanofibers: broadening applications for conducting polymers. *Chemical Society Reviews* 46:1510–1525
[43] Bhadra S, Khastgir D, Singha NK, Lee JH. 2009. Progress in preparation, processing and applications of polyaniline. *Progress in Polymer Science* 34:783–810
[44] Lei H, Pan N, Wang X, Zou H. 2018. Facile synthesis of phytic acid impregnated polyaniline for enhanced U(VI) adsorption. *Journal of Chemical & Engineering Data* 63:3989–3997
[45] Lei H, Pan N, Zou H, Wang X, Tuo X. 2023. Hollow self-assembled hybrid framework based on phytic acid for U(VI) capture from highly acidic aqueous media. *Chemical Engineering Journal* 472:144919
[46] Zhao X, Chen D, Zhang N, Shi M, Hu W, et al. 2024. Biodegradable chitosan-zirconium composite adsorptive membranes for potential arsenic (III/V) capture electrodialysis. *International Journal of Biological Macromolecules* 256:128356
[47] Yin Q, Liu J, Zhong Z, Zhang Y, Zhang F, et al. 2023. Synthesis of phytic acid-modified chitosan and the research of the corrosion inhibition and antibacterial properties. *International Journal of Biological Macromolecules* 253:126905
[48] Peng Q, Jin T, Wang C, Qian Y. 2024. Phytic acid-modified carboxymethyl cellulose hydrogel for uranium adsorption from aqueous solutions. *International Journal of Biological Macromolecules* 256:128545
[49] Ansari MZ, Ali Ansari S, Parveen N, Alam MW, Kim SH. 2025. The role of high-entropy materials and d-band center adjustments in supercapacitor development. *Journal of Energy Storage* 131:117535
[50] Ren Q, Xia H, Wang Y, Lv J, Yuan D, et al. 2024. Novel malonamide-amidoxime bifunctional polymers decorated graphene oxide/chitosan electrode for enhancing electrosorptive removal of uranium(VI). *Separation and Purification Technology* 330:125292
[51] Liu Y, Zhou L, Xie Y, Ao X, Ouyang J, et al. 2024. Enhancing U(VI) removal by using biomass-derived hierarchical porous carbon/α-MnO_2 nano fiber composites as high hybrid capacitance electrodes for capacitive deionization. *Process Safety and Environmental Protection* 182:948–959
[52] Shehzad H, Chen J, Shuang MT, Liu Z, Farooqi ZH, et al. 2024. Insights into electro-assisted and selective adsorption of U(VI) using hierarchical porous and activated biocarbon from lotus pods/2D-MoS_2/polypyrrole composites through capacitive deionization. *Process Safety and Environmental Protection* 181:354–366
[53] Endrizzi F, Leggett CJ, Rao L. 2016. Scientific basis for efficient extraction of uranium from seawater. I: Understanding the chemical speciation of uranium under seawater conditions. *Industrial & Engineering Chemistry Research* 55:4249–4256
[54] Krot AD, Tararushkin EV, Trigub AL, Vlasova IE, Kalmykov SN. 2025. Uranium coordination on clay surface at nanoscale: integration of EXAFS data and *ab initio* molecular dynamics. *Applied Clay Science* 274:107863
[55] Wang F, Zhang J, Jia S, Chen X, Cheng Z. 2025. A review of modification strategies and applications for hydrated salts: insights from energy storage materials encapsulation technology. *Renewable and Sustainable Energy Reviews* 223:115998
[56] Liu Y, Zhou L, Ouyang J, Ao X, Shuang M, et al. 2024. Electrodeposition nanofabrication of carboxylated carbon nanotubes/α-MnO_2 nanorods/polypyrrole composites as high hybrid capacitance electrodes for efficient U(VI) electrosorption. *Separation and Purification Technology* 334:125989
[57] Jin M, Huang X, Wang Z, Chan V, Hu J, et al. 2023. Mn, N co-doped carbon nanospheres for efficient capture of uranium(VI) via capacitive deionization. *Chemosphere* 342:140190
[58] Hu Q, Wang D, Liang J, Liu Z, Li J. 2024. Porous carbonized N-doped MOF-199 modified with MWCNTs for the deionization of uranium(VI). *Separation and Purification Technology* 330:125494
[59] Jiao R, Chen Z, Zeng S, Wang D, Li J. 2023. Electrosorption of uranium(VI) by sulfonic acid-decorated FeOOH nanorods. *Journal of Environmental Chemical Engineering* 11:111275
[60] Zhang Y, Zhou J, Wang D, Cao R, Li J. 2022. Performance of MXene incorporated MOF-derived carbon electrode on deionization of uranium(VI). *Chemical Engineering Journal* 430:132702
[61] Tang W, Li D, Zhang X, Guo F, Cui C, et al. 2023. A modified freezing-casted conductive hierarchical porous polymer composite electrode for electrochemical extraction of uranium from water. *Separation and Purification Technology* 319:124087
[62] Zhao X, Chen D, Shi M, Zhao R. 2024. Anchoring chitosan/phytic acid complexes on polypyrrole nanotubes as capacitive deionization electrodes for uranium capture from wastewater. *International Journal of Biological Macromolecules* 270:132491
[63] Guo D, Yan C, Huang B, Jin T, Liu Z, et al. 2025. Combining electrosorption and electrochemical reduction mechanisms for uranium removal using 1,2,3,4-butane tetracarboxylic acid-modified MIL-101: an in-depth exploration of uranyl–adsorbent interactions. *Inorganic Chemistry* 64:1777–1787
[64] Huang J, Huang B, Jin T, Liu Z, Huang D, et al. 2022. Electrosorption of uranium(VI) from aqueous solution by phytic acid modified chitosan: an experimental and DFT study. *Separation and Purification Technology* 284:120284
[65] Yang S, Luan Z, Li W, Cheng X, Ye Z, et al. 2024. Two-dimensional sp^2 carbon-conjugated COFs electrode for efficient electro-adsorption of uranium. *Separation and Purification Technology* 330:125378
[66] Li Q, Zhou J, Xu Y, Jin Z, Zhou H. 2025. Interface-driven electronic modulation enhances US coordination in carbon-confined Co-Mo sulfide heterojunctions for electrochemical uranium extraction. *Chemical Engineering Journal* 519:164881
[67] Yang S, Yan C, Huang B, Jin T, Guo D, et al. 2025. PBTCA-modified self-crosslinked chitosan gels for efficient electrosorption of uranium from wastewater. *Desalination* 612:118984